respectively. CCDC-179137 (**2**) and CCDC-179138 (**3**) contain the supplementary crystallographic data for this paper. These data can be obtained free of charge via www.ccdc.cam.ac.uk/conts/retrieving.html (or from the Cambridge Crystallographic Data Centre, 12, Union Road, Cambridge CB2 1EZ, UK; fax: (+44) 1223-336-033; or deposit @ccdc.cam.ac.uk).

[6] M. Gerloch, F. E. Mabbs, *J. Chem. Soc. A* **1967**, 1598 – 1608.

[7] R. H. Heistand II, A. L. Roe, L. Que, Jr., *Inorg. Chem.* **1982**, *21*, 676 – 681.

[8] $\tau = (\beta - \alpha)/60$, $\beta > \alpha$. A. W. Addison, T. N. Rao, J. Reedijk, J. van Rijn, G. C. Verschoor, *J. Chem. Soc. Dalton Trans.* **1984**, 1349 – 1356.

[9] A. E. True, A. M. Orville, L. L. Pearce, J. D. Lipscomb, L. Que, Jr., *Biochemistry* **1990**, *29*, 10847 – 10854.

[10] D. C.-T. Siu, A. M. Orville, J. D. Lipscomb, D. H. Ohlendorf, L. Que, Jr., *Biochemistry* **1992**, *31*, 10443 – 10448.

[11] H. Fujisawa, M. Uyeda, Y. Kojima, M. Nozaki, O. Hayaishi, *J. Biol. Chem.* **1972**, *247*, 4414 – 4421.

[12] The iron-bound hydroxide ligand in 3,4-PCD is protonated to an aqua ligand around pH 6.0 with binding of sulfate ion to the iron: M. W. Vetting, D. A. Argenio, L. N. Ornston, D. H. Ohlendorf, *Biochemistry* **2000**, *39*, 7943 – 7955.

[13] P. Coggon, A. T. McPhail, F. E. Mabbs, V. N. McLachlan, *J. Chem. Soc. A* **1971**, 1014 – 1019.

[14] Complexes **3** and **4** exhibit only one set of signals for phenolate protons (**3**: $\delta = 89.9$ and 58.3, **4**: $\delta = 73.7$ and 42.2) in CD_2Cl_2 at 296 K. This is due to a fast exchange between two fluxional isomers resulting from pseudorotation of the salen ligand **1**; extreme line broadening has been observed at low temperature.

[15] The EPR spectrum of **2** showed other ferric high-spin signals at $g = 6.7$, 5.2, and ca. 2. This indicates a more axial iron center ($E/D \sim 0.03$), which is probably a six-coordinated form resulting from binding of ethanol to **2** at 4 K.

[16] L. Que, Jr., J. D. Lipscomb, J. M. Wood, *Biochim. Biophys. Acta* **1977**, *485*, 60 – 74.

Micro/Nanoengineering of the Self-Organized Three-Dimensional Fibrous Structure of Functional Materials

Xiang Y. Liu* and Prashant D. Sawant

Supramolecular functional materials[1] with 3D fibrous network structures formed by interconnecting nanosized fibrils have important applications in, for example, drug delivery, coatings, lithography, catalyst supporters, scaffolds for tissue engineering, the engineering of nanostructural and self-supporting porous materials, and novel separation for macromolecules.[1–5] Macroscopic properties, in particular, the rheological properties of supramolecular functional materials are determined by the microstructure of fibrous networks. The fibrous networks with permanent interconnections will effectively entrap and immobilize liquid in the meshes and promote the formation of self-supporting rigid gels, which possess the elastic properties of ideal solids and the viscosity properties of a Newtonian liquid.[2,4,6] In contrast, systems consisting of nonpermanent or transient interconnecting (such as entangled) fibrils or needles reveal only viscous weak gels at low concentrations.[2]

Significant efforts have been devoted to the identification of novel systems with a desirable microscopic structural organization that can enable formation of such functional materials.[2,4,5] One such route includes the screening of a large number of potential gelator/solvent systems capable of forming 3D self-organized interconnecting fibrous networks.[2,4–7] However, through the lack of suitable of materials, screening is very difficult. Thus for a given system, it would be extremely desirable to construct or engineer interconnecting 3D fiber networks at the micro- or nanolevel with such organization that materials with the expected functionalities can be created. We aim to illustrate a completely new approach to engineering such materials by constructing permanent 3D interconnecting nanofibrous networks from a system consisting of separate fibers.

The materials to be examined were obtained by dissolving lanosta-8,24-dien-3β-ol:24,25-dihydrolanosterol (L/DHL), 56:44 molar ratio, Sigma) in diisooctylphthalate (DIOP, 99% purity, Aldrich) at approximately 125 °C, and then cooling the sample to approximately room temperature.

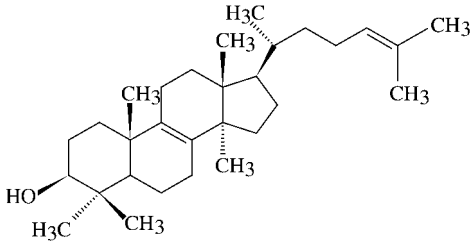

L/DHL

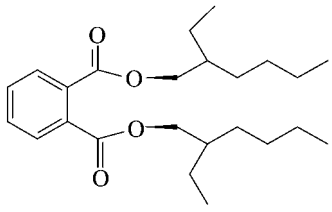

DIOP

Scanning electronic microscopy (SEM) coupled with a CO_2 super-critical fluid-extraction technique (Thar Design) was applied to examine the micro- and nanostructure of the fibrous networks. The latter technique is used to remove the liquid captured in the networks without disturbing their overall structure.[8]

An opaque and viscous paste was obtained on cooling the aforementioned system (10 wt% L/DHL) to room temperature (Figure 1a, inset). The system consists of only nonbranched fibers or needles, which are in temporary contact with each other (Figure 1a).

Our strategy is to create networks with permanent interlinking from such a system. An additive, ethylene/vinyl acetate copolymer (EVACP, $(C_4H_6O_2 \cdot C_2H_4)_n$, $M_W =$ ca. 100000, 40% in vinyl acetate), is introduced to achieve the microstructured architecture. Surprisingly, under identical

[*] Prof. Dr. X. Y. Liu, Dr. P. D. Sawant
Interfaces and Micro/Nanostructures Lab
Department of Physics
National University of Singapore
2 Science Drive 3, Singapore 117542 (Singapore)
Fax: (+65) 777-6126
E-mail: phyliuxy@nus.edu.sg

  0044-8249/02/4119-3641 $ 20.00+.50/0

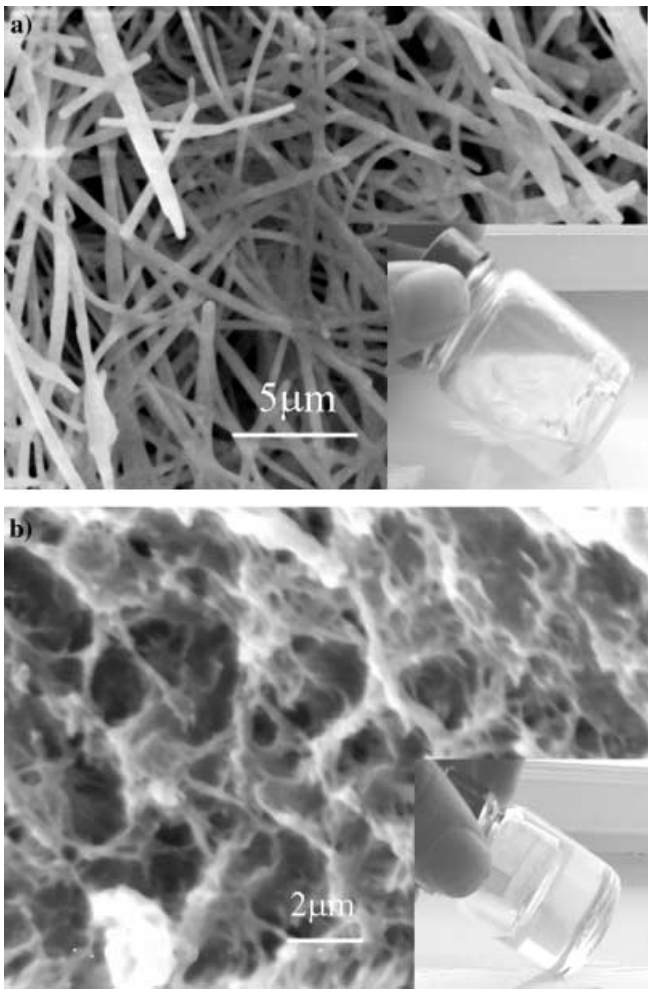

Figure 1. a) Separate fibers occurring in the 10 wt % L/DHL/DIOP system. An opaque paste is obtained, as shown in the inset. b) Interconnected fiber networks in the 10 wt % L/DHL/DIOP system after adding EVACP. A clear and tough gel was obtained, as shown in the inset.

conditions to those described above, a tiny amount of EVACP (0.006 wt %) is sufficient to create interconnecting self-organized microscopic networks of nanofibers in the L/DHL/DIOP system (Figure 1b), which results in the formation of a solid and self-supporting gel (Figure 1b; neat vinyl acetate exerts no effect on the branching).

To investigate the influence of such a structural change on macroscopic properties, the rheological properties of the system were measured (Figure 2). Instantaneous measurement of the applied stress and the resultant strain allows the calculation of the storage modulus (G', which describes the elastic property) and the loss modulus (G'', which describes the viscosity), which, in turn, gives the complex modulus G^* ($G^* = [(G')^2 + (G'')^2]^{1/2}$).[7,9–11]

Figure 2a displays the change in G^* as a function of time for the L/DHL/DIOP system. The value of G^* increases abruptly at $t \geq t_g$ (t_g = gelation time), which indicates the formation of L/DHL fibrils. The value of G^* reaches its maximum G^*_{max} when the formation of the fiber network is complete, which occurs as $t \rightarrow \infty$. In comparison with the control sample, the G^*_{max} value is almost doubled after a small amount of EVACP is added. (Similar changes were also obtained for G' and G'',

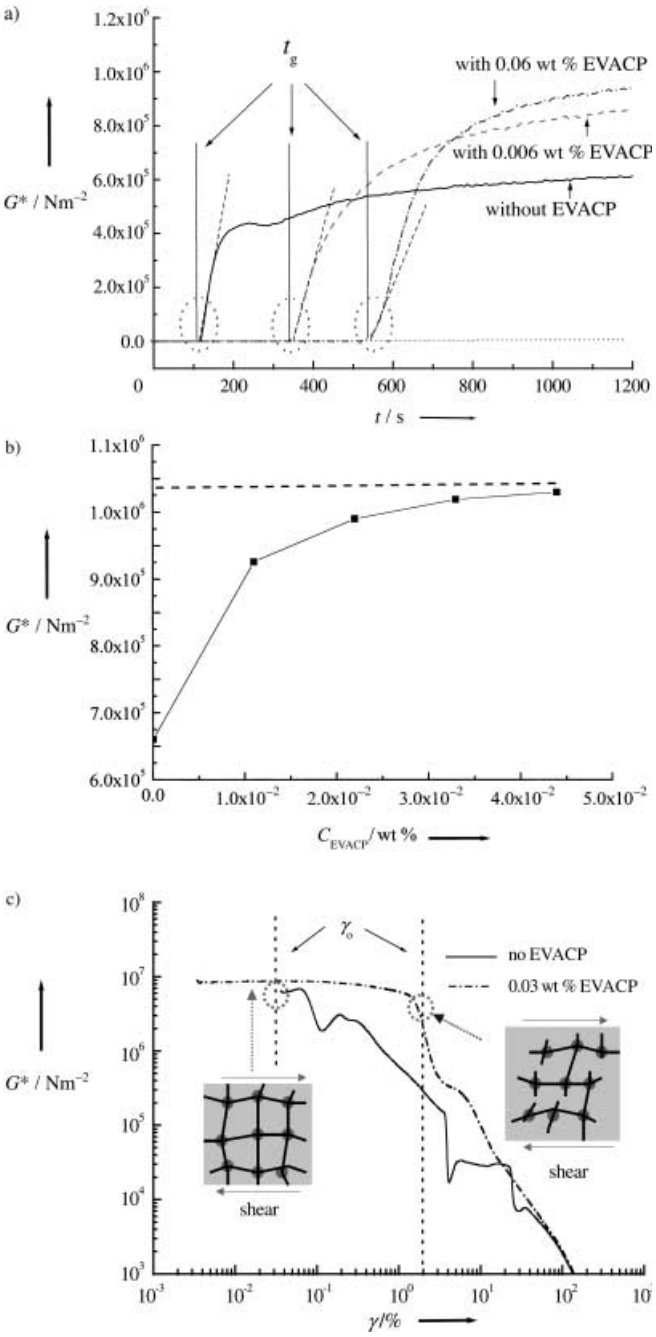

Figure 2. Changes in the rheological properties of the 10 wt % L/DHL/DIOP system, both with and without EVACP, as functions of time and strain.[19] a) Dependence of the magnitude of complex modulus G^* on time. The amplitude of the oscillations was controlled to obtain a 0.1 % strain in the sample. (Under this strain limit, the structure of supramolecular materials will not be destroyed by the measurements.) The maximal G^* is almost doubled after adding EVACP. The slope of $G^* \sim t$ ($= dG'/dt$) at $t \rightarrow t_g$ ($t > t_g$) represents the growth rate of L/DHL fibrils. b) Dependence of the magnitude of complex modulus G^* on the concentration of EVACP (C_{EVACP}) for the above system. c) Dependence of the storage modulus G' on strain. The linearity limit γ_o is enhanced almost 100 times after adding EVACP.

respectively.) The change in G^* as a function of EVACP concentration (C_{EVACP}) is given in Figure 2b. As indicated, the value of G^* increases drastically at low C_{EVACP} values, which is as a consequence of greater interconnectivity between L/

  0044-8249/02/4119-3642 $ 20.00+.50/0

DHL fibers. As C_{EVACP} increases further, G^* gradually reaches a constant level. This can be attributed to fine adjustment of the interconnecting fiber networks. The SEM micrographs suggest that the branching period of L/DHL fibers changes from approximately 1.2 to 0.8 μm as C_{EVACP} varies from 0.006 to 0.1 %. Within the same concentration range, the thickness of the fibers varies between approximately 30 and 60 nm, which is much thinner than that of L/DHL fibers without EVACP (approximately 800 nm).

Figure 2c shows the change in G' at various oscillating strain amplitudes (γ) at an angular frequency (ω) of 0.2π rad s^{-1}. The strain corresponds to the deformation of the networks caused by the applied shear stress. The value of G' remains constant (linear) at small strains and decreases abruptly when γ exceeds a certain value, γ_o. The onset of nonlinearity (decrease in G') at γ_o indicates bond breakage within the networks.[12] Figure 2c indicates that the addition of EVACP leads to a significant enhancement (approximately 100 times) of the limit of linearity γ_o. Since our experiments show that EVACP itself has no direct impact on the G' or γ_o values, the changes of G^*, G', and γ_o must be attributed to the establishment of 3D interconnecting fiber networks.

To explore the network-promotion mechanism of EVACP, one must first understand the cross-linking mechanism. It is believed[2,4] that the formation of nanofibers of small molecules such as L/DHL occurs through molecular self-assembly. This process implies that the fibrils have only low-dimensional or liquid-crystalline ordering, and the formation of networks should be controlled by diffusion.[2,4] However, X-ray diffraction (XRD) analysis show that L/DHL powders, needles, and 3D interconnecting fibrils have identical crystalline characteristics (Figure 3a). The formation of L/DHL needles and 3D interconnecting fibrils is, therefore, essentially controlled by a nucleation-growth process. According to 3D nucleation models[13] $\ln t_g$ is linearly dependent on $1/(\Delta\mu/kT)^2$. Here, $\Delta\mu$ is the difference in chemical potential between L/DHL molecules in the fibril and in the liquid phase, and can be given by Equation (1).

$$\frac{\Delta\mu}{kT} \cong \frac{\Delta H_{diss}}{k T_{eq} T}(T_{eq} - T) \quad (1)$$

ΔH_{diss} denotes the molar dissolution enthalpy of the nucleating phase, T_{eq} and T are the equilibrium temperature for a given concentration and the experimental temperature, respectively, and k is the Boltzmann constant.

On the basis of the above results (Figure 3) and the "trimmed Cayley tree" structure (Figure 1b), we propose that propagation of the interconnecting network of L/DHL after adding EVACP proceeds as follows: primary nucleation→fiber growth→crystallographic mismatch branching→fiber growth→crystallographic mismatch branching, etc. (Figure 4c).[14] One of the key steps to building self-organized interconnecting fiber networks is the so-called crystallographic mismatch branching (CMB)[14] induced by EVACP. This process occurs when crystal layers on the tips of the growing fibrils exert a certain degree of structural mismatch with respect to the crystallographic orientation of the parent fibers. This situation leads to the formation of new daughter fibers on the tips of the parent fibers (Figure 4b).

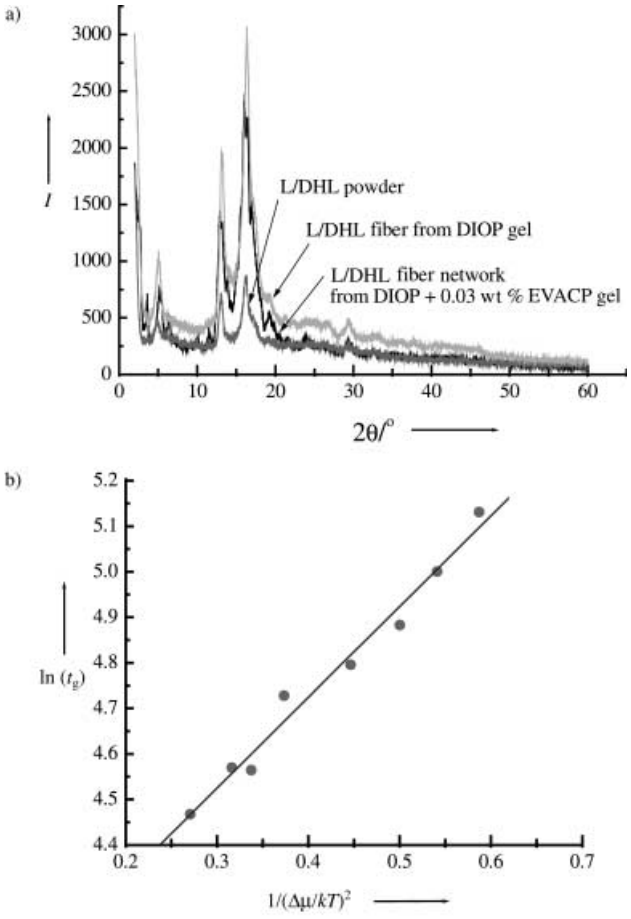

Figure 3. a) X-ray diffraction analysis for L/DHL crystalline powders and fibrils. All forms have crystalline order and an identical structure. b) Plots of $\ln t_g \sim 1$ versus $(\Delta\mu/kT)^2$ for the 10 wt % L/DHL/DIOP system. A linear relationship is obtained, which indicates the control of nucleation during fibril formation.[13]

The formation of sharp crystalline needles or fibers arises from the rapid growth of the tips, which implies that the kinetic resistance of sharp fibril tips along the fibril axis is very low in comparison with other directions,[13,15] and corresponds to a very low step-free energy (that is, the energy required to create a step at the crystal surface).[15] Consequently, the growth of L/DHL fibrils is very likely to be controlled by either 2D nucleation "birth-and-spread growth" or "rough-growth" mechanisms.[13,15] The birth-and-spread mechanism involves growth along the fibril axis by growing new crystal layers on top of an existing layer through 2D nucleation (Figure 4a).[13]

For the growth of separate needlelike fibrils, integration of L/DHL molecules into the crystal structure of fibrils at the tip surface is much more rapid than the transport of molecules from the bulk to the surface.[13,15] It follows that all growth units transported to the tip surface will be incorporated into the tip instantly.[13] Therefore, the concentration of deposited material at the surface of the tips is very close to the equilibrium concentration (or supersaturation $\Delta\mu/kT \rightarrow 0$).

For a crystalline system, the probability of heterogeneous nucleation, which leads to the occurrence of new fibrils, depends on both the structural match between the substrate

  0044-8249/02/4119-3643 $ 20.00+.50/0

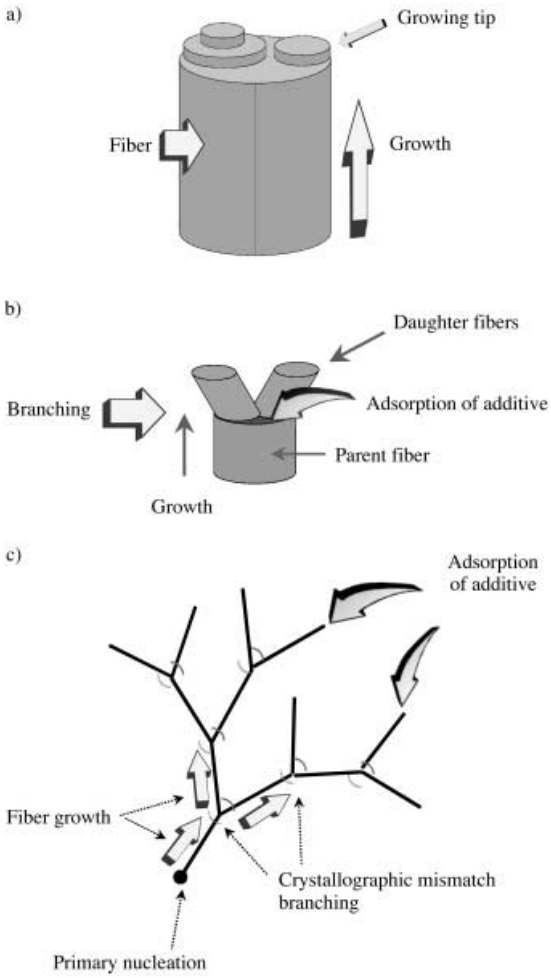

Figure 4. a) Growth of L/DHL fibrils controlled by the birth-and-spread two-dimensional nucleation mechanism.[13,22] This process can take place at low supersaturation values, and correspondingly the structure of the new layers occurring at the tip of the fibrils exactly matches that of the crystal surface. b) The adsorption of EVACP causes mismatch nucleation at the tip of growing fibril, which leads to crystallographic mismatch branching. c) The formation of interconnecting fiber networks.

and the nucleating phase, as well as supersaturation.[13] It is of note that the surface of existing fiber tips can also be a perfect substrate for self- or auto-epitaxial nucleation and growth.[13b,16] For the growth of L/DHL needles, the deposition of new layers on the existing surface of growing tips requires a perfect structural match at very low levels of surface supersaturation (Figure 4a).[13] As the surface supersaturation increases, the tendency for a mismatch of new layers on the existing surface of growing tips (Figure 4b) increases because of the lowering of the mismatch nucleation barrier.[13] If structural mismatch occurs, new fiber branches will emerge from the tips of existing fibers, which leads to CMB (Figure 4b).

EVACP is an agent that will selectively adsorb on certain surfaces of organic crystals.[17] The molecules can strongly adsorb on the tip of growing fibrils or the surface of foreign particles. As shown in Figure 2a,the value of t_g, which is proportional to the induction time of primary nucleation, changes from 1.2×10^2 to 3.4×10^2 and 5.4×10^2 s upon addition of 0.006 and 0.06 wt % EVACP, respectively. These results suggest that the primary nucleation of L/DHL, which normally initiates from foreign particles,[13] is suppressed by the adsorption of EVACP onto the surface of the particles.[13,15] More importantly, the adsorption of EVACP on the tip of growing fibrils will hinder significantly the integration of surface L/DHL molecules into the crystal[18] and, consequently, reduce the growth rate of the fibers. It can be seen from Figure 2a that the growth rate of the fibrils in the axial direction, R_g, changes from 9C to 3.3C and 1.2C (C = constant) when 0.006 and 0.06 wt % EVACP are added, respectively (see the legend of Figure 2a and ref. [23] for details). Consequently, the surface supersaturation is greatly enhanced to a level close to the bulk supersaturation.[13] As mentioned above, high surface supersaturation promotes the formation of new fibrils on the tip of the parent fibril (Figure 4b), which leads to the onset of CMB. The experiments verify that the correlation between the branching distance and supersaturation $1/(\Delta\mu/kT)$ can be described quantitatively by the CMB mechanism when branching occurs. [19]

Otsubo[20] reported that silica particle suspensions also form 3D networks on addition of polyacrylamide. The network is formed by the adsorption of one polymer chain onto two or more existing particles, which binds them together. In this case, the polymer molecules serve as bridging materials in the formation of the 3D network, and adsorption onto the surface of particles is an irreversible process. In contrast, the EVACP introduced into the L/DHL/DIOP system promotes the branching of lanosterol fibrils by affecting the kinetics of fiber formation, rather than through direct involvement by bridging different existing fibrils. This process completely alters the topology of the fiber networks, and leads to the formation of the Cayley tree type of 3D interconnecting network (Figures 1c and 4c). Therefore, in comparison with the bridging mechanism, additive-induced CMB requires a much lower quantity of polymer than the previous case (at least two magnitudes lower).[21] The formation of 3D interconnecting nanofiber networks of L/DHL by the addition of EVACP is thermally reversible since the branching process is kinetically controlled. This is in contrast to the thermally irreversible 3D network formed by the bridging of polyacrylamide, and exemplifies the differences between these systems.[20]

It is noticeable that the adsorption of additives on the growing tips may reduce the anisotropy of needlelike growth, and result in tip-splitting as a consequence of instability at the corners.[15,22] The branching in our case is a special type of 3D nucleation (Figure 4d), whereas tip-splitting is essentially a diffusion-control growth process. As an important distinction, the split tips and the parent fiber belong to the same crystal, whereas the daughter fibers and the parent crystal in CMB belong to different crystallites (Figure 1b).

In conclusion, we have constructed a 3D interconnecting fibrous network of a supramolecular functional material at the micro/nanoscale level, by utilizing a "branching creator", EVACP. This novel approach can enable the creation and engineering of interconnecting 3D nanofiber networks with a desired structure and significantly modified rheological properties. Our experiments show that the architecture of the

  0044-8249/02/4119-3644 $ 20.00+.50/0

microstructure is controlled by the newly identified crystallographic mismatch branching mechanism, rather than molecular self-assembly.

Received: February 19, 2002 [Z18736]

[1] a) M. J. Mio, J. S. Moore, *MRS Bull.* **2000**, *25*, 36 – 41; b) D. Derossi, K. Kajiwara, Y. Osada, A. Yamauchi, *Polymer Gels: Fundamentals and Biomedical Applications*, Plenum, New York, **1991**; c) J. M. Guenet, *Thermoreversible Gelation of Polymers and Biopolymers*, Academic Press, London, **1992**; d) D. Kremer, G. Lagaly, *Prog. Colloid. Polym. Sci.* **1996**, 102 – 107; e) R. J. R. Corriu, D. Leclercq, *Angew Chem.* **1996**, *108*, 1524 – 1540; *Angew. Chem. Int. Ed. Engl.* **1996**, *35*, 1420 – 1436; f) M. I. Reetz, *Adv. Mater* **1997**, *9*, 943 – 954.

[2] a) P. Terech, R. G. Weiss, *Chem. Rev.* **1997**, *97*, 3133 – 3159; b) U. Beginn, S. Keinath, M. Möller, *Macromol. Chem. Phys.* **1998**, *199*, 2379 – 2348.

[3] L. Brunsveld, B. J. B. Folmer, E. W. Meijer, *MRS Bull.* **2000**, *25*, 49 – 53.

[4] J. H. van Esch, B. L. Feringa, *Angew. Chem.* **2000**, *112*, 2351 – 2354; *Angew. Chem. Int. Ed.* **2000**, *39*, 2263 – 2266.

[5] T. Oya, T. Enoki, A. U. Grosberg, S. Masamune, T. Sakiyma, Y. Tekeoka, K. Tanaka, G. Wang, Y. Tilmaz, M. S. Feld, R. Dasari, T. Tanaka, *Science* **1999**, *286*, 1543 – 1545.

[6] P. C. Hiemenz, and R. Rajagopalan, *Principles of Colloid and Surface Chemistry*, Marcel Dekker, New York, **1997**, pp. 145 – 192.

[7] P. Terech, D. Pasquier, V. Bordas, C. Rossat, *Langmuir* **2000**, *16*, 4485 – 4494.

[8] J. R. Ilzhoefer, R. J. Spontak, *Langmuir* **1995**, *11*, 3288 – 3291.

[9] P. Meakin, *Phys. Rev. A* **1983**, *27*, 1495 – 1507.

[10] D. S. Graff, L. M. Sander, *Phys. Rev. E* **1993**, *47*, R2273—R2276.

[11] O. van Cantfort, A. Brasseur, B. Michaux, R. Pirard, J. P. Pirard, A. J. Lecloux, *Faraday Discuss.* **1995**, *101*, 265 – 274.

[12] W. H. Shih, W. Y. Shih, S. I. Kim, J. Liu, I. A. Aksay, *Phys. Rev. A* **1990**, *42*, 4772 – 4779.

[13] a) X. Y. Liu, *J. Chem. Phys.* **2000**, *112*, 9949 – 9955; b) X. Y. Liu, *Langmuir* **2000**, *16*, 7337 – 7345; c) X. Y. Liu in *Advances in Crystal Growth Research* (Eds.: K. Sato, K. Nakajima, Y. Furukawa), Elsevier, Amsterdam, **2001**.

[14] a) X. Y. Liu, P. D. Sawant, *Appl. Phys. Lett.* **2001**, *79*, 3518 – 3520; b) X. Y. Liu, P. D. Sawant, *Adv. Mater.* **2002**, *14*, 421 – 426.

[15] A. A. Chernov, *Modern Crystallography III–Crystal Growth*, Springer, Berlin, **1984**.

[16] a) X. Y. Liu, C. S. Strom, *J. Chem. Phys.* **2000**, *112*, 4408 – 4411; b) C. S. Strom, X. Y. Liu, M. Wang, *J. Phys. Chem. B* **2000**, *104*, 9638 – 9646.

[17] P. Bennema, X. Y. Liu, K. Lewtas, R. D. Tack, J. J. M. Rijpkema, K. J. Roberts, *J. Cryst. Growth* **1992**, *121*, 679 – 696.

[18] a) X. Y. Liu, E. S. Boek, W. J. Briels, P. Bennema, *Nature* **1995**, *374*, 342 – 345; b) X. Y. Liu, E. S. Boek, W. J. Briels, P. Bennema, *J. Chem. Phys.* **1995**, *103*, 3747 – 3754; c) X. Y. Liu, *Phys. Rev. B* **1999**, *60*, 2810 – 2817.

[19] X. Y. Liu, P. D. Sawant, unpublished results.

[20] Y. Otsubo, *Adv. Colloid Interface Sci.* **1994**, *53*, 1 – 32.

[21] X. Y. Liu, K. Maiwa, K. Tsukamoto, *J. Chem. Phys.* **1997**, *106*, 1870 – 1879.

[22] D. A. Kessler, J. Koplik, H. Levine, *Adv. Phys.* **1988**, *37*, 255 – 339.

Exceptional Rate Enhancements and Improved Diastereoselectivities through Chelating Diamide Coordination in Intramolecular Alkene Hydroaminations Catalyzed by Yttrium and Neodymium Amido Complexes**

Young Kwan Kim and Tom Livinghouse*

The catalyzed intramolecular hydroamination of carbon–carbon multiple bonds is one of the most important methods for the synthesis of nitrogen heterocycles.[1] Of the variety of metal-based catalysts for this transformation, complexes of the lanthanides appear uniquely well suited for effecting chemoselective alkene hydroaminations under mild reaction conditions.[2,3] The vast majority of the complexes that have found utility for this purpose are comparatively air- and moisture-sensitive metallocene derivatives. We recently disclosed that simple amido derivatives of the Group 3 metals corresponding to the formula $[Ln\{N(TMS)_2\}_3]$ (**1**; Ln = lanthanide, TMS = trimethylsilyl) are competent catalysts for intramolecular alkene hydroamination.[4] Herein we show that catalytic activity can be dramatically increased and cyclization diastereoselectivity improved by coordination of the active metal center to simple chelating diamide ligands (Scheme 1).

As part of our previous study,[4] we noted that the addition of representive amino alkenes to catalytic quantities

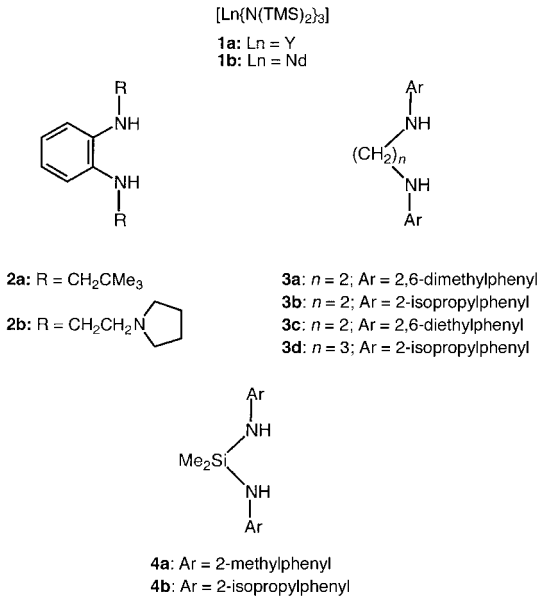

Scheme 1. Ligands for lanthanide complexes **1** employed in this study.

[*] Prof. Dr. T. Livinghouse, Y. K. Kim
Department of Chemistry
Montana State University
Bozeman, MT 59717 (USA)
Fax: (+1) 406-994-5407
E-mail: livinghouse@chemistry.montana.edu

[**] Financial support for this research was provided by the National Science Foundation. T.L. would like to thank Professor John E. Bercaw for technical advice during the early phases of this program.

Supporting information for this article is available on the WWW under http://www.angewandte.org or from the author.

  0044-8249/02/4119-3645 $ 20.00+.50/0